Heliyon 10 (2024) e23947

Contents lists available at ScienceDirect

Heliyon

journal homepage: www.cell.com/heliyon

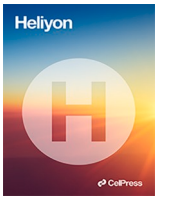

Integrated analysis of necroptosis related gene signature to predict clinical outcomes, immune status and drug sensitivity in lower grade Glioma

Xiqi Hu [a], Yanan Ma [b], Ying Xia [a], Bo Liu [c,*]

[a] Department of Neurosurgery, Central South University Xiangya School of Medicine Affiliated Haikou Hospital, Haikou, 570100, China
[b] Hainan Affiliated Hospital of Hainan Medical University, Haikou, 570100, China
[c] Department of Neurosurgery, Xiangya Hospital, Central South University, Changsha, 410000, China

ARTICLE INFO

Keywords:
Necroptosis
Immune infiltration
Tumor microenvironment
Risk score model
LGG (lower grade glioma)

ABSTRACT

Background: The treatment of lower grade gliomas (LGG) is currently the most challenging dilemma in the management of intracranial tumors. Necroptosis is a type of programmed cell death that is closely associated with tumor progression, However, the role of necroptosis related genes in LGG is not yet well elucidated.

Methods: Online databases were used to obtain gene expression and clinical information. After gene differential expression analysis, a risk score model based on prognostic differentially expressed necroptosis-related genes (DENGs) were constructed to predict prognosis for LGG patients. The validity of the risk score model was then assessed with Kaplan-Meier survival curve. The prognostic DENGs included in the risk score model were then subjected to gene expression analysis, functional enrichment analysis, consensus clustering analysis, and single cell sequencing analysis. Finally, we investigated the correlation of the risk score and immune infiltration in LGG tumor microenvironment and drug sensitivity for LGG patients in different risk groups.

Results: A survival risk score model was constructed based on seven prognostic DENGs, which demonstrated satisfactory performance in predicting the prognosis of LGG patients. According to functional enrichment analyses, these seven DENGs may play a regulatory role in LGG tumorigenesis through several immune and metabolic pathways. LGG patients could be categorized into two clusters with distinct prognosis and clinicopathologic characteristics based on the expression of seven DENGs. Single-cell sequencing analysis demonstrated that the DENG signature was differentially expressed in various types of cells in LGG and may play a vital role in oncogenesis. Additionally, drug sensitivity analysis suggested that the seven-gene signature could guide clinical medication for LGG patients.

Conclusion: Our study developed a reliable necroptosis-related signature to predict the prognosis of LGG patients. This gene signature may also help estimate immune status and anti-cancer drug sensitivity in LGG patients. Our findings may pave the way to enhance our understanding of necroptosis in LGG.

* Corresponding author.
E-mail address: liuboxy@csu.edu.cn (B. Liu).

https://doi.org/10.1016/j.heliyon.2023.e23947
Received 13 May 2023; Received in revised form 5 November 2023; Accepted 16 December 2023
Available online 18 December 2023

1. Introduction

Gliomas are the most common tumors in the human central nervous system (CNS), with an estimated prevalence of 80 % and a high mortality and disability rate [1]. Lower grade glioma (LGG) is categorized based on the neoplasm's histological appearance and genetic mutations [2]. Traditionally, LGG has been classified as WHO grade II and III gliomas. It has been considered a chronic benign disease that primarily affects young people and has minimal impact on the quality of life for most patients, particularly those with oligodendrogliomas, as it rarely causes severe neurological deficits other than seizures. However, recent studies have revealed that LGG continues to grow at an average rate of 4–5 mm per year [3]. Untreated symptomatic and incidental tumors eventually progress to malignancy, resulting in a more complex disease course, reduced quality of life, and ultimately shorter survival for most patients [4].

Although conventional surgical resection, radiation therapy combined with immunotherapy, and novel electric field therapy have moderately improved the prognosis of glioma patients, the overall prognosis remains poor due to the heterogeneity of LGG and epigenetic mutations in intratumor molecules. These mutations include mutations in isocitrate dehydrogenase (IDH) and epidermal growth factor receptor, co-deletion of 1p19q, and methylation of the O6-Methylguanine-DNA Methyltransferase (MGMT) promoter [5]. Furthermore, the WHO 2021 CNS Tumor Classification System underscores the necessity of classifying gliomas based on histological and molecular genetic features for clinical diagnosis and outcome prediction. The classification system emphasizes the significance of tumor molecular subtyping and prognostic biomarkers for diagnosis and treatment [1]. Thus, a comprehensive understanding of the molecular mechanisms of glioma relapse and progression, the discovery of new biomarkers, and the exploration of novel predictive models for improved diagnosis, treatment, and prognosis are urgently required.

It is well known that programmed cell death, namely apoptosis and necroptosis, plays a significant role in embryonic development and tissue homeostasis [6]. Necroptosis has been identified as an alternative form of cell death that shares characteristics with both necrosis and apoptosis. Necroptosis is associated with various neurological pathologies [7], involving mechanisms such as neuronal cell degeneration, blood-brain barrier damage, axonal degeneration, disruption of RNA metabolism, and defects in axonal transport leading to neurological demise. Necroptosis plays a pivotal role in processes like tumorigenesis, metastasis, treatment response, prognosis, and immunity [8,9]. Studies involving glioma cells have demonstrated a tumor-suppressive effect through the induction of necroptosis [10]. Furthermore, several studies have indicated a close connection between necroptosis and immune infiltration within the glioma microenvironment [11,12]. Necroptotic cells can deliver antigens and pro-inflammatory cytokines to dendritic cells (DCs) and activate cytotoxic $CD8^+$ T cells [13]. Upon phagocytosis of necroptotic cells, phagocytes can release pro-inflammatory cytokines, triggering a robust immune response [14], which can foster angiogenesis, facilitate cancer cell proliferation, and expedite cancer metastasis, thereby promoting tumor development [8,15]. As a result, necroptosis may play dual roles in glioma, acting as both a tumor suppressor and a promoter.

Therefore, conducting a comprehensive investigation into the mechanism of necroptosis within the tumor microenvironment and analyzing its potential immunological implications could contribute to the understanding of necroptosis in the development of LGG. These insights might pave the way for new potential immunotherapeutic strategies for the treatment of LGG in the future.

2. Methods

2.1. Data collecting

RNA-sequencing data and clinical information for LGG were obtained from The Cancer Genome Atlas (TCGA) database and the Chinese Glioma Genome Atlas (CGGA) database. The combined gene expression data of TCGA (tumor) and GTEx (normal brain), with batch effects eliminated, were downloaded from the UCSC Xena data portal and utilized for the screening of differentially expressed genes (DEGs) [16]. A list of necroptosis-related genes was obtained from the Kyoto Encyclopedia of Genes and Genomes (KEGG) (hsa04217). LGG samples with incomplete survival information were excluded.

2.2. Screening for differentially expressed genes

We utilized the "DESeq2," "edgeR," and "limma" packages to identify differentially expressed genes (DEGs) between LGGs and normal brain tissues. DEGs were identified using a threshold of adjusted p-values <0.05 and an absolute log2-fold change >1. The common intersection of necroptosis-related genes and the DEGs identified by the three algorithms were subjected to subsequent analyses. These genes, referred to as differentially expressed necroptosis-related genes (DENGs) in this study, underwent further analysis.

2.3. Construction and evaluation of the risk score model and the nomogram

We first conducted univariate Cox regression analysis to identify DENGs with significant prognostic value. Subsequently, we employed the least absolute shrinkage and selection operator (LASSO) Cox regression analysis to identify the prognostic DENGs that were then included in the risk score model ($p < 0.01$). Next, we examined the expression of the prognostic DENGs and clinicopathological features across different risk score groups. Univariate and multivariate Cox regression analyses were performed, integrating the risk score and relevant clinicopathological features, to evaluate and compare their prognostic prediction abilities. We also examined the expression of prognostic DENGs between normal brains and LGGs. Additionally, we conducted Kaplan-Meier survival analysis to assess patient survival and utilized receiver operating characteristic (ROC) analysis to further validate the model's

prediction specificity and sensitivity using the TCGA and CGGA datasets, respectively. For more in-depth analysis, we evaluated the risk score model's capability to predict patient survival within each subgroup of clinical characteristics. Moreover, to enhance prognosis prediction, we constructed a nomogram-based linear prognostic model by integrating the risk score with clinical characteristics.

2.4. Further analysis of the prognostic DENGs

We carried out functional enrichment analyses to delve deeper into the potential functional properties of the DENGs identified in the risk score model. Subsequently, to achieve further subtype classification of LGG, we conducted consensus clustering analysis. The correlation between these prognostic DENGs and tumor subtypes, high and low-risk scores, and clinical risk factors was analyzed through heatmap visualization.

To explore the distribution of gene expression across distinct cell types in LGG, we conducted single-cell RNA sequencing (scRNA-seq) analysis using the CGGA scRNA dataset. The scRNA-seq data underwent processing through the "seurat" package for analysis, followed by downsizing and grouping via principal component analysis (PCA) and t-distributed stochastic neighbor embedding (tSNE). Each cell was annotated using the "scCATCH" package to provide contextual information [17].

2.5. Immune infiltration and drug sensitivity analyses

Single-sample gene set enrichment analysis (ssGSEA) was employed to estimate the infiltration of 22 immune cell types and assess immune pathway activity. To further investigate the correlation between the risk score and the immune microenvironment in LGG, six different algorithms: TIMER, CIBERSORT, quanTIseq, MCP-counter, xCELL and EPIC were utilized. These algorithms were used to evaluate immune cell infiltration disparities between the high and low-risk score groups. Lastly, we employed the "oncoPredict" package in conjunction with the Genomics of Drug Sensitivity in Cancer (GDSC2) database (https://gdsc-combinations.depmap.sanger.ac.uk/) to predict drug sensitivity (IC50 value) across different risk groups [18].

2.6. Statistical analysis

Statistical analysis in the study was conducted using R 4.12 software. All R packages used in the study are open access and free to

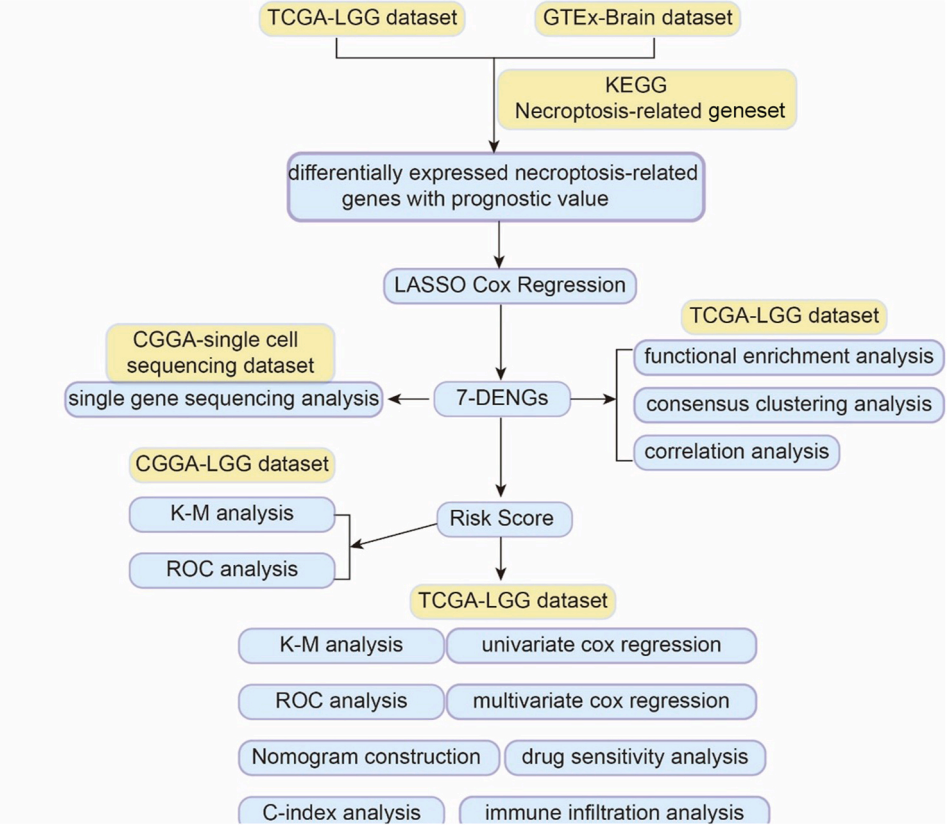

Fig. 1. Study flow chart.

use. The log-rank test, *t*-test, and Kruskal-Wallis test were applied as appropriate. A p-value less than 0.05 was considered statistically significant, unless otherwise indicated.

3. Results

3.1. Data access

The research process of this study is depicted in the flowchart (Fig. 1). A total of 149 necroptosis-related genes were extracted from the KEGG database. For this study, 530 and 443 LGG samples with genomic and clinicopathological data were incorporated from the TCGA and CGGA databases, respectively. Additionally, 1148 normal brain samples with RNA sequencing data were retrieved from the GTEx database.

3.2. Differentially expressed genes

We identified 10,026 down-regulated genes and 3367 up-regulated genes between normal brain and LGG tissues using the "DESeq2″ package (Fig. 2A). Employing the "EdgeR" package, we detected 9616 down-regulated genes and 4279 up-regulated genes (Fig. 2B). Similarly, through "limma" package analysis, we pinpointed 4158 down-regulated genes and 4552 up-regulated genes (Fig. 2C). By overlapping the results of the three DEG analyses, we ultimately identified 2777 up-regulated and 3919 down-regulated DEGs (Fig. 2D). Among the 6696 DEGs, we discovered 23 out of the 149 necroptosis-related genes exhibiting differential expression between LGG and normal brain tissue. These 23 genes were subsequently utilized in further analyses.

3.3. The risk score model and the nomogram

Through LASSO Cox regression analysis, we identified seven prognostic DENGs along with their risk coefficients, which were then utilized to construct a risk predicting model for LGG (Fig. 3A and B). The risk score was calculated based on the expression levels of the seven prognostic DENGs (model DENGs) and their corresponding risk coefficients using the following formula: risk score = (0.08) * co-expression of H2AFX + (−0.16) * co-expression of H2AFY2 + (−0.02) * co-expression of BID + (−0.02) * co-expression of MAPK10 + (−0.14) * co-expression of VDAC2 + (0.06) * co-expression of CASP8 + (−0.31) * co-expression of GLUD1. The bar chart illustrated the

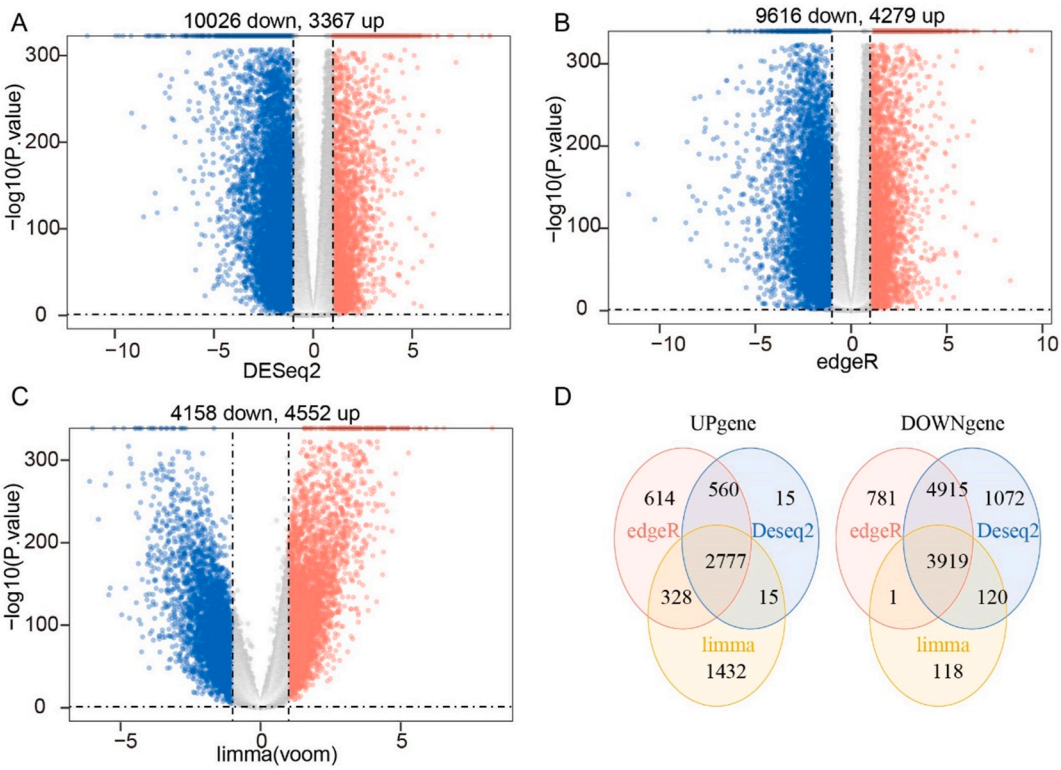

Fig. 2. Identification of differentially expressed genes.
(A, B, C) Volcano plots of differentially expressed genes screened by DESeq2, edgeR, and limma package. (D) Venn diagrams showing the overlapping of up-regulated genes and down-regulated genes.

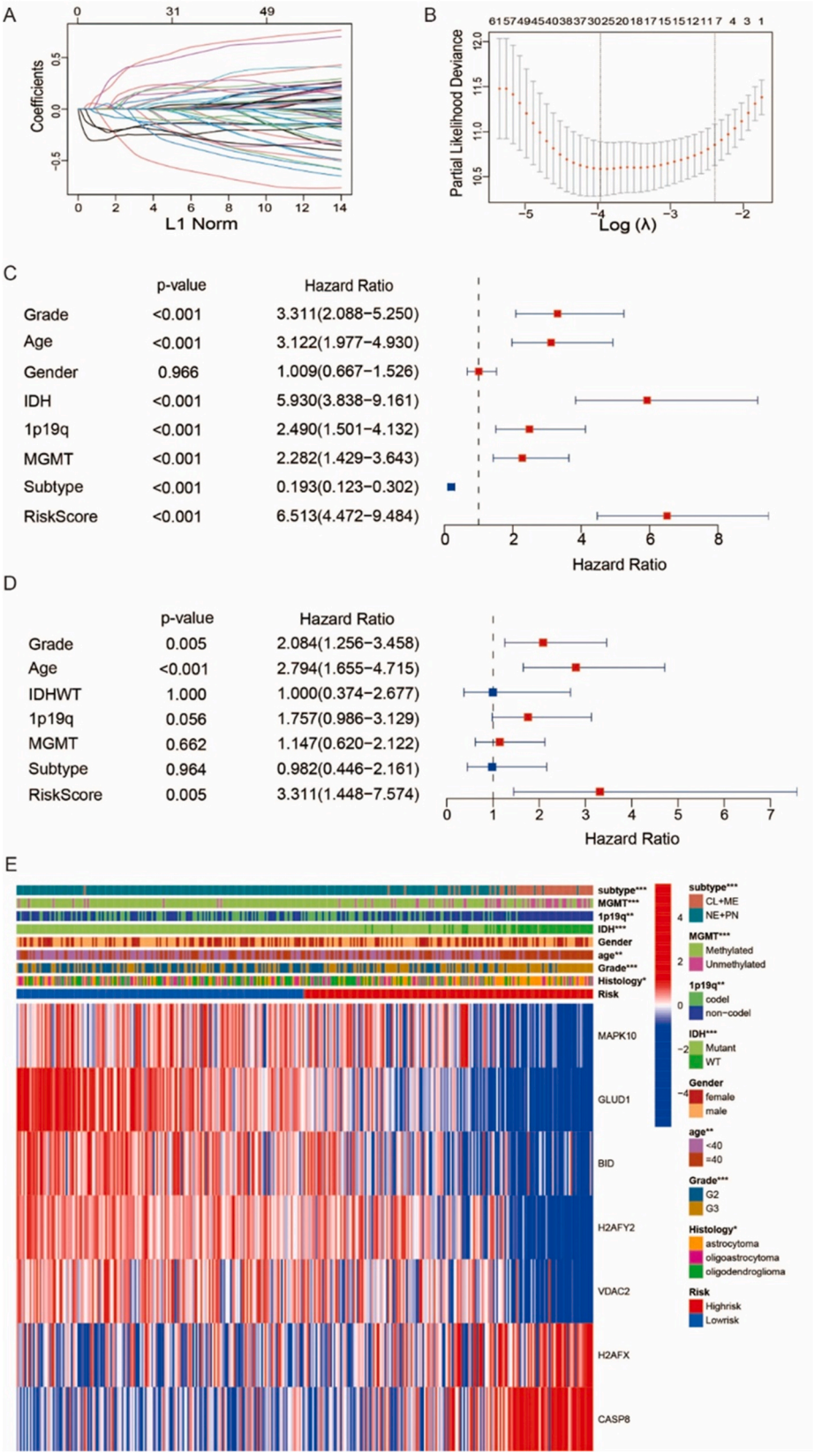

(caption on next page)

Fig. 3. Construction and evaluation of the risk score model in LGG. (A, B) The prognostic signature constructed by the LASSO Cox regression. (C) Univariate Cox regression analysis in the TCGA dataset. (D) Multivariate Cox regression analysis in the TCGA dataset. (E) Heatmap depicting the expression of the seven model DENGs and the corresponding clinicopathological features in high-risk and low-risk groups.(*$p < 0.05$, **$p < 0.01$, ***$p < 0.001$).

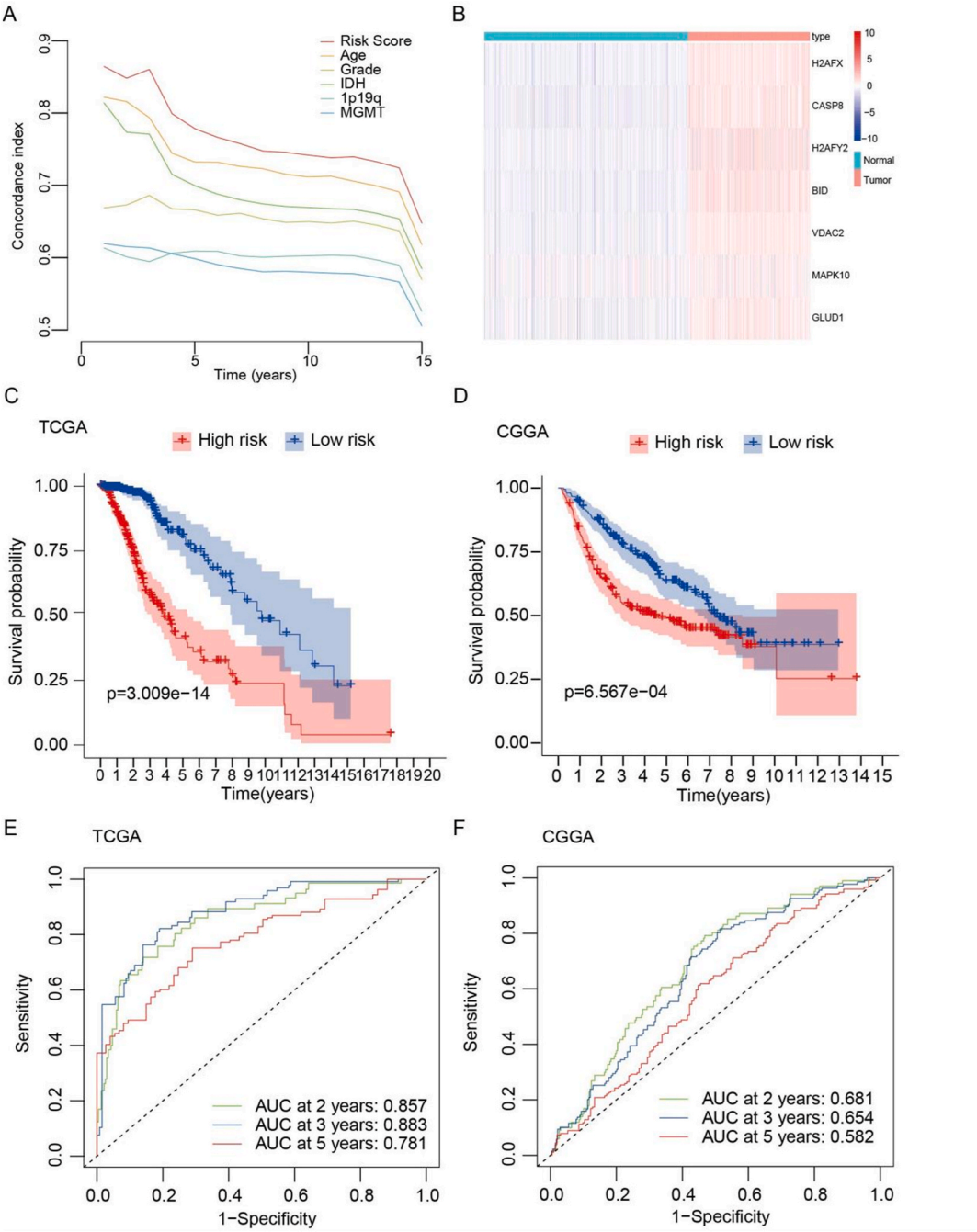

Fig. 4. Assessment of the risk score model in the TCGA and CGGA datasets. (A) C-index of the risk score and clinical prognostic factors. (B) Heatmap illustrating the expression of the seven model DENGs in normal brain sample and in LGG sample. (C, D) Kaplan-Meier survival curves of patients with high and low-risk scores in the TCGA and CGGA dataset. (E, F) Area under ROC curves for predicting LGG at 2, 3 and 5 year in the TCGA and CGGA dataset.

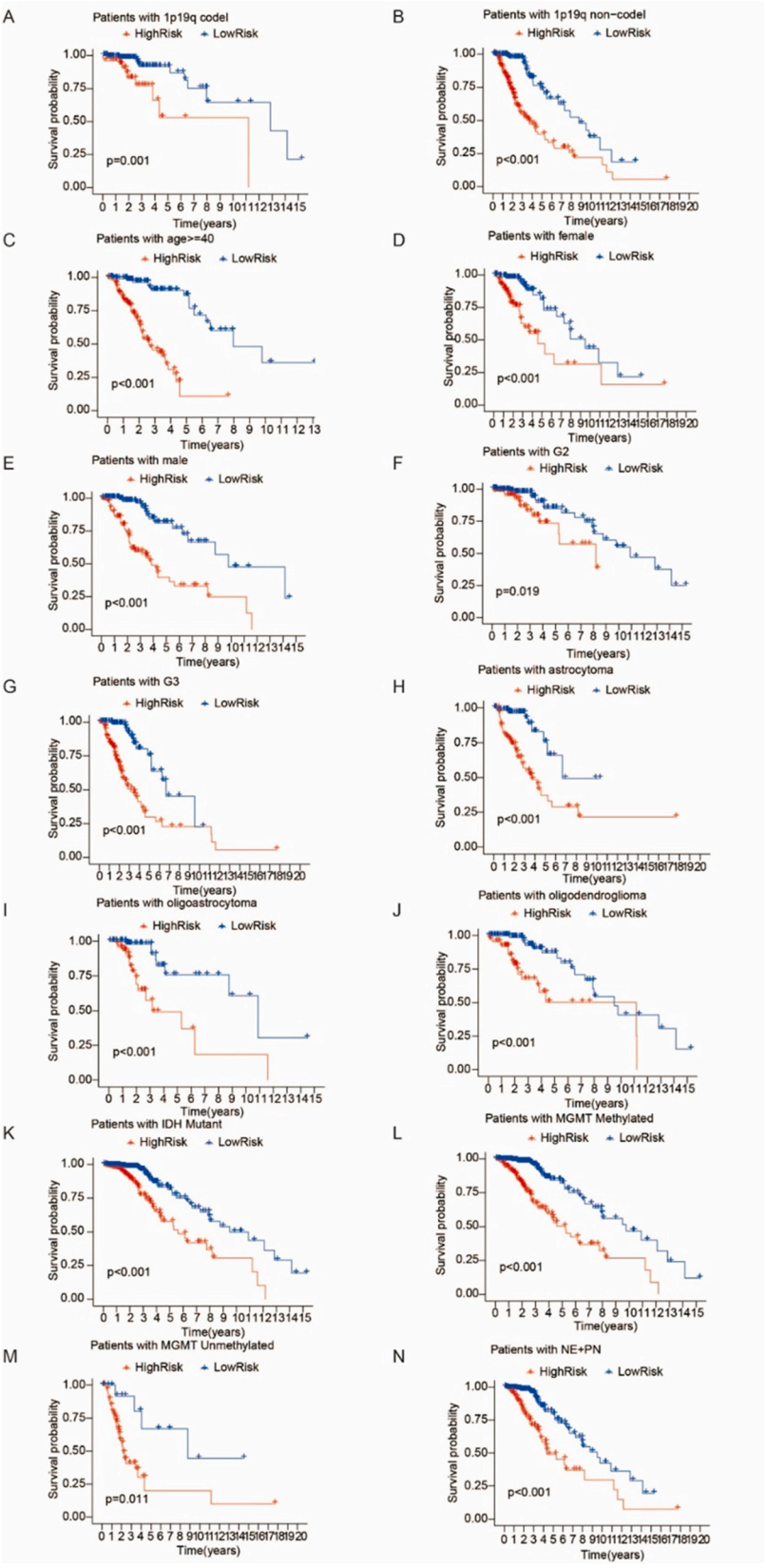

(caption on next page)

Fig. 5. Stratified survival analysis of patients within high and low-risk groups. (A) Patients with 1p19q codeletion. (B) Patients with 1p19q non-codeletion. (C) Patients of age ≥40 years (D) Female patients. (E) Male patients. (F) Patients of WHO grade 2. (G) Patients of WHO grade 3. (H) Patients with astrocytoma. (I) Patients with oligoastrocytoma. (J) Patients with oligodendroglioma. (K) Patients with IDH mutant. (L) Patients with MGMT promoter methylated. (M) Patients with MGMT promoter unmethylated. (N) Patients with NE + PN subtypes.

comparison of the model DENGs' expression between normal brain and LGG samples (Fig. 4B).

Univariable Cox regression analysis demonstrated a statistically significant association between survival in LGG patients and WHO grade, age, IDH, 1p19q, MGMT status, molecular subtype, and the risk score, with the exception of gender ($p = 0.966$) (Fig. 3C). Upon inclusion of these variables in multivariate Cox regression analysis, both WHO grade and age, along with the risk score model, maintained significant associations with survival (Fig. 3D). The heatmap depicted the expression patterns of the model DENGs and corresponding clinicopathological features across the two risk groups (Fig. 3E). In comparison to clinical risk factors, the risk score demonstrated superior predictive power for survival compared to WHO grade, age, IDH, 1p19q, and MGMT (Fig. 4A). As evident from

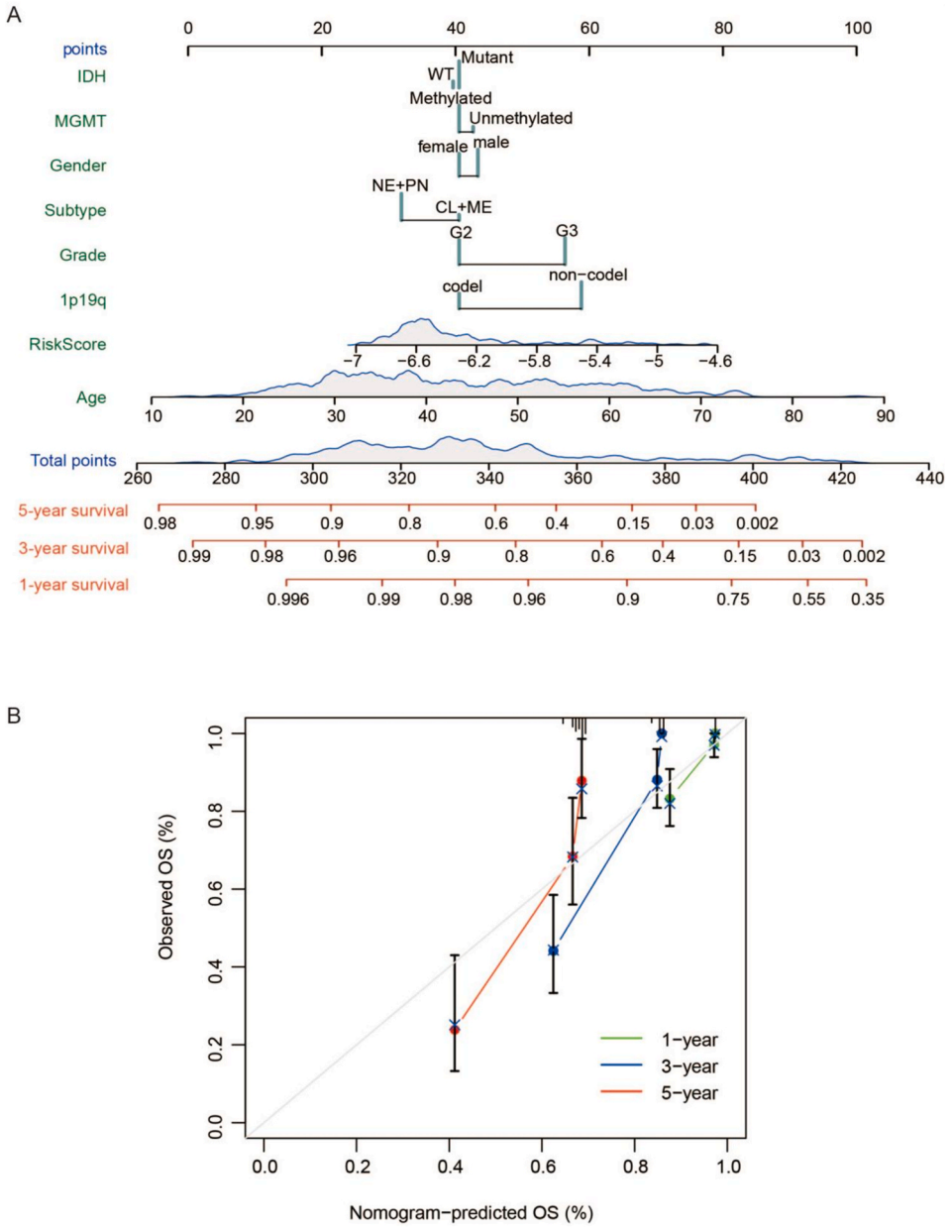

Fig. 6. Construction and evaluation of the nomogram based on clinical prognostic features and risk score. (A) Nomogram for predicting survival at 1, 3 and 5 years in patients with LGG. (B) Calibration plots of the nomogram for predicting the survival probability at 1, 3 and 5 year.

the Kaplan-Meier survival curve and ROC curve, the risk score model exhibited excellent survival discrimination within both the TCGA and CGGA LGG cohorts (Fig. 4C–F), thereby indicating a robust and accurate predictive performance for survival outcomes.

The risk score model also exhibited the ability to predict survival outcomes in LGG patients across various categories, including different 1p19q status (Fig. 5A and B), WHO grades (Fig. 5F and G), pathology classes (Fig. 5H–J), MGMT status (Fig. 5L and M), and individuals aged over 40 years (Fig. 5C), as well as those with IDH mutation and neural & proneural subtypes (NE + PN) (Fig. 5N). However, the risk score model proved ineffective in predicting survival for individuals with IDH wild-type (WT), individuals younger than 40 years, and individuals with classical & mesenchymal subtypes (Fig. S1).

Subsequently, we constructed a nomogram to improve the estimation of LGG survival probability. This was achieved by integrating IDH, MGMT, gender, molecular subtype, age, WHO grade, 1p19q status, and the risk score (Fig. 6A). The calibration curves revealed strong agreement between observed and predicted outcomes for the nomogram, signifying the nomogram's effective capacity to predict survival (Fig. 6B).

3.4. Functional enrichment analyses

Gene Ontology (GO) analysis demonstrated enrichments across biological process (BP), cellular component (CC), and molecular function (MF) categories. Terms such as pattern specification process, regionalization, embryonic organ development, anterior or posterior pattern specification, and embryonic skeletal morphogenesis were observed to be enriched within the BP category. The CC category showed enrichment in the transcriptional regulator complex, while the MF category revealed enrichment in DNA-binding transcriptional activator activity within the context of LGG (Fig. 7A and B). In addition, KEGG pathway enrichment analysis unveiled that the model DENGs were primarily associated with pathways such as complement and coagulation cascades, ubiquinone biosynthesis, and the phenylalanine pathway (Fig. 7C and D).

3.5. Clustering based on the model DENGs

Based on the expression levels of the model DENGs, LGG patients were effectively classified into two distinct clusters (Fig. 8A–D). Notably, patients in cluster 1 displayed a significantly improved prognosis in comparison to those in cluster 2 (Fig. 8E). The correlation

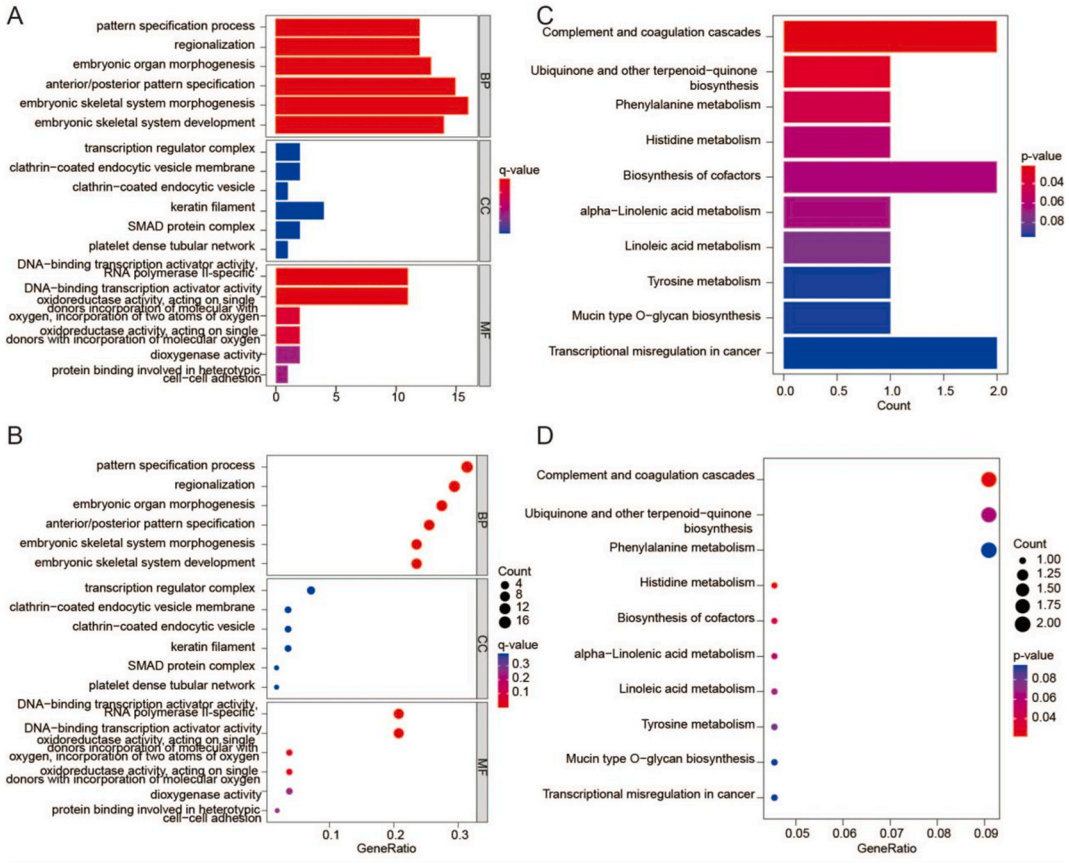

Fig. 7. Functional enrichment analyses of the seven model DENGs. (A, B) The top significant GO terms of functional enrichment analysis. (C, D) The top significant KEGG pathways of functional enrichment analysis.

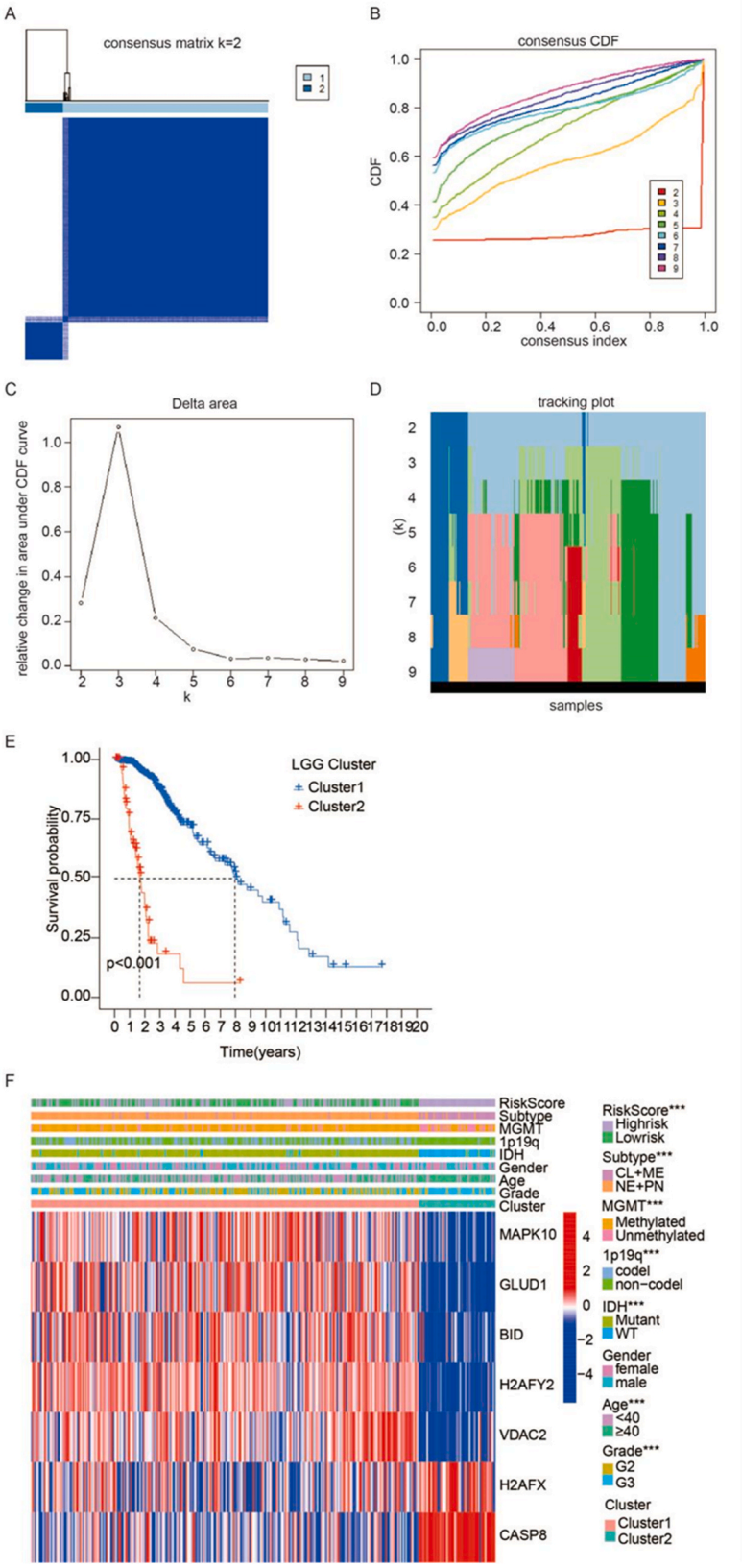

(caption on next page)

Fig. 8. Consensus clustering based on the seven DENGs and correlation of DENGs with clinical features. (A–D) LGG patients could be well divided into two distinct necroptosis-related clusters. (E) The Kaplan-Meier survival curves for cluster 1 and 2. (F) Heatmap displaying the expression of the seven model DENGs and clinical features in two necroptosis-related clusters.(*$p < 0.05$, **$p < 0.01$, ***$p < 0.001$).

between pertinent clinical features across the two clusters was visually presented in a heatmap, which emphasized that patients in cluster 1 were more likely to exhibit features such as methylated MGMT, 1p19q codeletion, younger age, lower WHO grade, mutant IDH, NE + PN subtype, and a lower risk score (Fig. 8F).

3.6. Expression of model DENGs at the single-cell level

The scRNA-seq data of LGG single cells underwent dimensionality reduction, resulting in the identification of seven distinct cell populations. These populations were subsequently annotated into five cell types: oligodendrocytes, T cells, macrophages, astrocytes, and microglial cells (Fig. 9A and B). The model DENGs were differentially expressed across these cell types (Fig. 9C–I). Specifically, H2AFX and MAPK10 exhibited high expression levels in oligodendrocytes and macrophages (Fig. 10A and E). BID (Fig. 10D), VDAC2 (Fig. 10F), and GLUD1 (Fig. 10G) demonstrated high expression across multiple cell types including oligodendrocytes, T cells, astrocytes, macrophages, and microglial cells. CASP8 displayed high expression in astrocytes and microglial cells (Fig. 10B), while H2AFY2 exhibited heightened expression in oligodendrocytes (Fig. 10C).

3.7. Immune infiltration analysis

To examine the correlation between the risk score and immune infiltration, we assessed scores for 16 immune cells and 13 immune-related pathways. Notably, significant differences were observed between patients in the two risk groups for several immune cell types, including dendritic cells (aDCs, iDCs, and pDCs), B cells, $CD8^+$ T cells, macrophages, various subsets of T helper cells (Th, Tfh, Th1, and Th2 cells), tumor-infiltrating lymphocytes (TILs) and regulatory T cells (Tregs) (Fig. 11A). Across all 13 immune-related pathways, activation levels were notably lower in the low-risk group compared to the high-risk group (Fig. 11B).

Moreover, we assessed immune infiltration between the high-risk and low-risk groups employing the TIMER, CIBERSORT, quanTIseq, MCP-counter, xCELL, and EPIC algorithms. The results were mostly consistent with the ssGSEA results that the high-risk group had higher levels of immune infiltration than the low-risk group (Fig. 12).

3.8. Drug sensitivity analysis

We predicted that 78 out of 199 anti-cancer drugs exhibited significantly enhanced effectiveness in high-risk or low-risk patients as compared to their respective counterparts ($p < 0.001$). For instance, topotecan (Fig. 13A), alpelisib (Fig. 13B), dabrafenib (Fig. 13C), entospletinib (Fig. 13D), gemcitabine (Fig. 13E), and trametinib (Fig. 13F) were predicted to demonstrate substantial sensitivity within the low-risk group. Conversely, alisertib (Fig. 13G), vinblastine (Fig. 13H), and lapatinib (Fig. 13I) were anticipated to exhibit significant sensitivity within the high-risk group. These findings suggest that the necroptosis-associated risk score could be employed in the selection of anti-cancer drugs.

4. Discussion

Necroptosis represents a novel programmed form of necrosis, with a growing number of genes linked to this process being identified. Interestingly, necroptosis shares mechanistic similarities with apoptosis and morphological resemblances to necrosis [6]. The traits of necroptosis within tumors have been progressively unveiled. In recent years, the genes associated with necroptosis have garnered escalating interest. These genes exhibit a dual effect, either promoting or impeding cancer progression, contingent upon the context [8].

Genotype constitutes a pivotal pathological trait of LGG that holds direct implications for prognosis and treatment determinations. Notably, the most frequently reported genotypes that exhibit strong correlations with LGG prognosis encompass IDH, 1p19q, and MGMT statuses [5,19]. Among these, IDH enzymes play a fundamental role in catalyzing the oxidative decarboxylation of isocitrate. Mutations within IDH result in the production of 2-hydroxyglutarate (2-HG) rather than α-ketoglutarate, which indirectly down-regulates vascular endothelial growth factor expression and ultimately inhibits tumor proliferation. Consequently, LGG patients with IDH mutations tend to demonstrate improved prognoses in comparison to those with IDH WT [20–22]. Furthermore, reports highlight that 1p19q co-deletions are most commonly observed in oligodendrogliomas and oligoastrocytomas [23]. Notably, in oligodendrogliomas, 1p19q co-deletions have exhibited predictive value in chemotherapy response and prognosis [24,25]. MGMT, a DNA repair enzyme, is associated with resistance to DNA alkylating therapies for glioma treatment, with MGMT promoter methylation present in 30–90 % of LGGs [26]. Multiple studies have demonstrated the linkage between MGMT promoter methylation, MGMT expression silencing, enhanced survival, and heightened chemotherapy sensitivity [27,28]. In summary, the IDH WT subtype, the MGMT promoter unmethylated subtype, and the 1p19q non-codeletion subtype generally coincide with less favorable prognoses. Consequently, to compare the prognostic gene associations related to necroptosis identified within this study with the prognoses of LGG patients, we included these classical genotypes alongside pertinent clinical characteristics.

This study involved the development of a necroptosis-related risk score model, focusing on the seven model DENGs, which

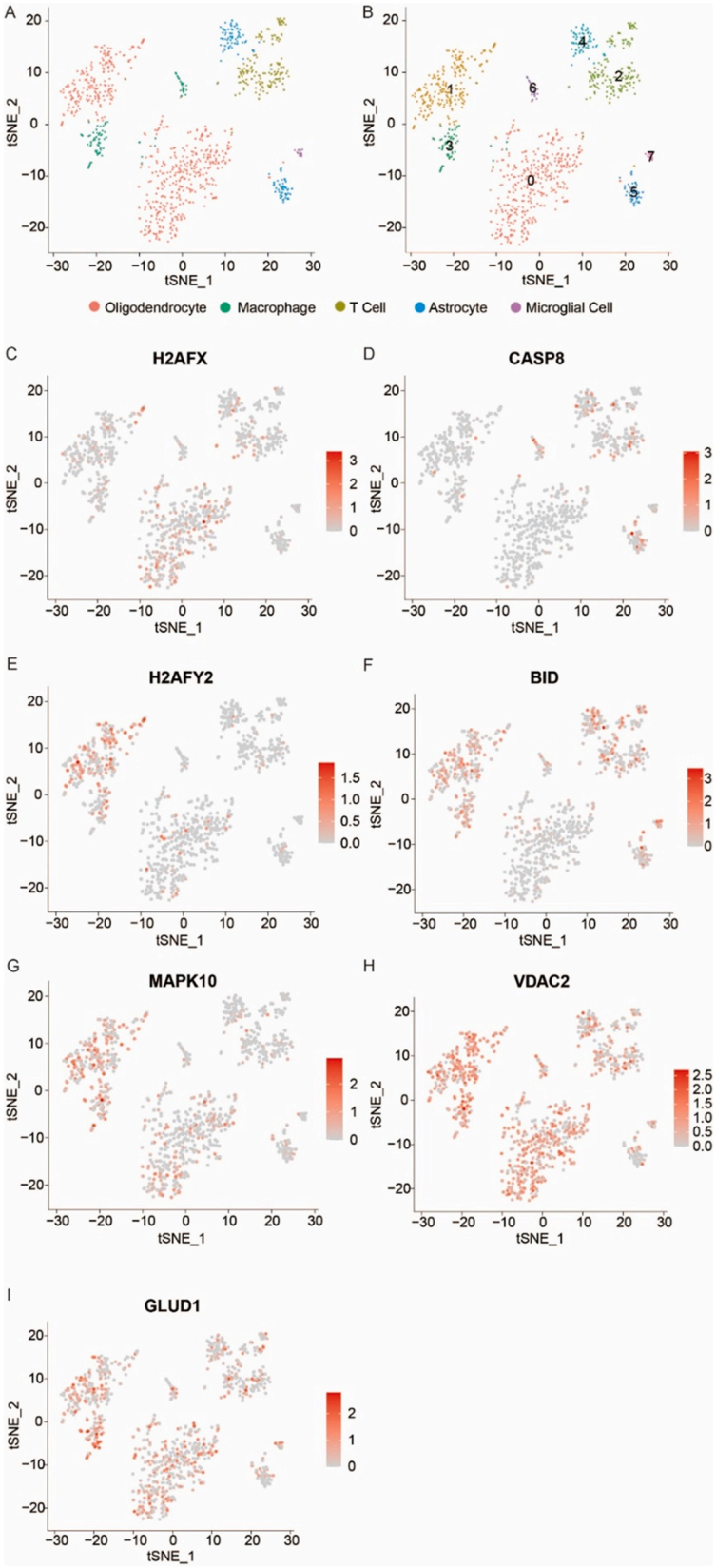

Fig. 9. scRNA-seq expression analysis. (A, B) Annotation of the cell types. (C–I) Expression of the seven model DENGs in five cell types.

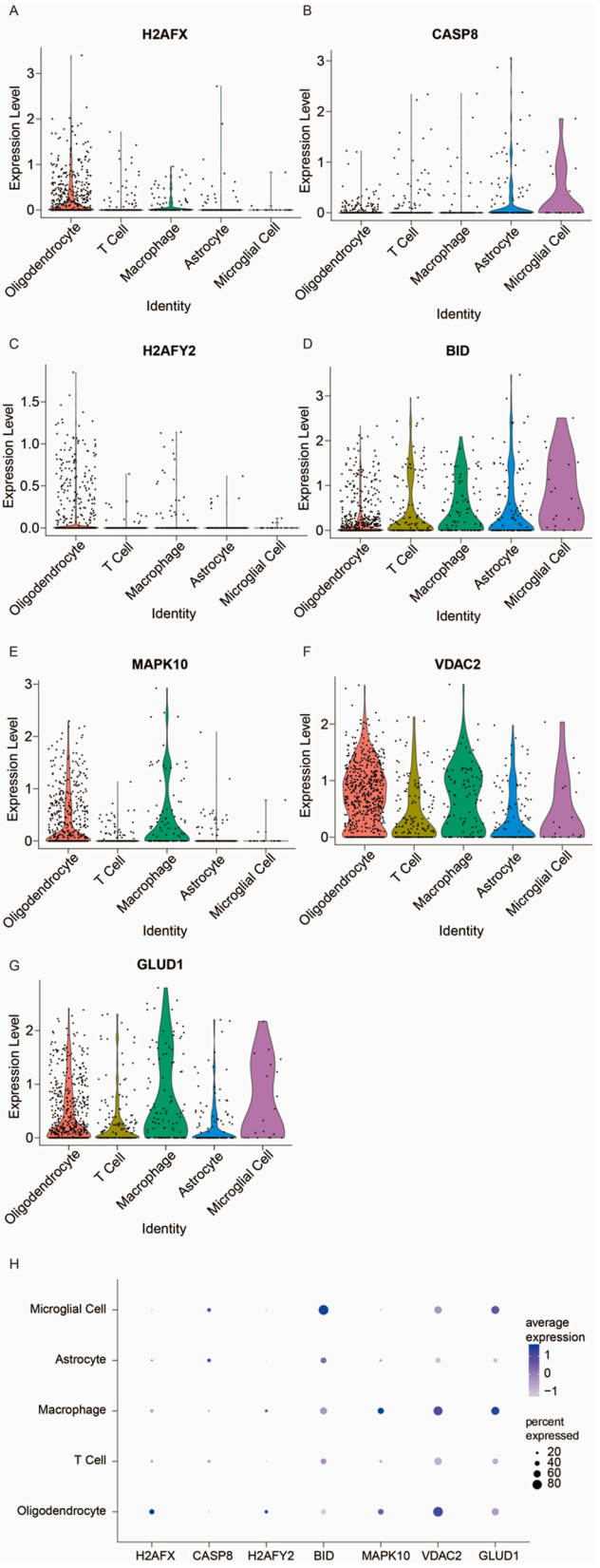

(caption on next page)

Fig. 10. Expression comparison of the model DENGs in each cell type. (A–G) Violin chart of the seven model DENGs in cell types. (H) Dot chart of the seven model DENGs in cell types.

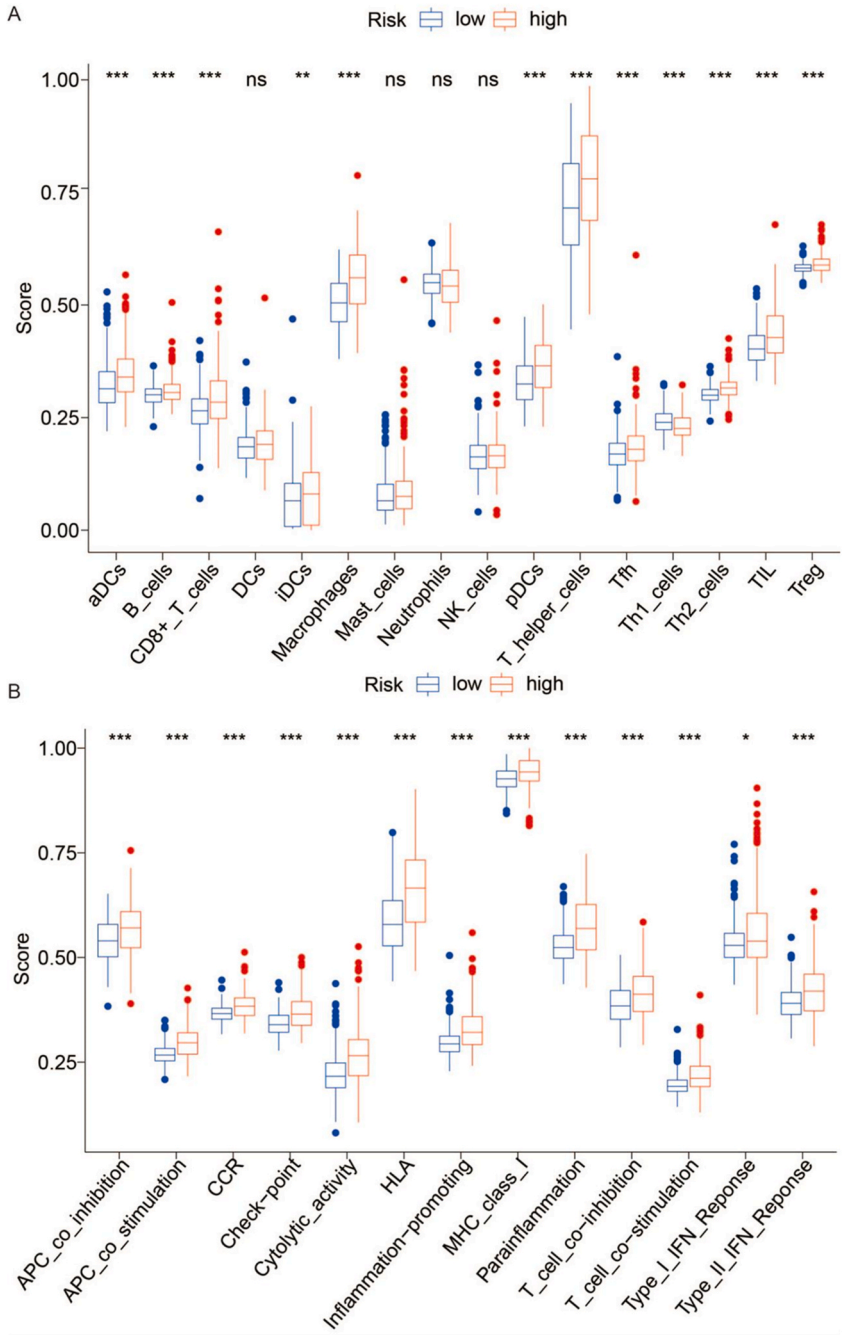

Fig. 11. ssGSEA analysis of immune infiltration within high- and low-risk groups. (A) 16 immune cells infiltration in hi- and low-risk groups (B) 13 immune-related pathways in hi- and low-risk groups.(*$p < 0.05$, **$p < 0.01$, ***$p < 0.001$).

demonstrated notable efficacy in predicting survival outcomes. The risk score showed concurrence with established prognostic factors associated with LGG, including molecular subtype, age, WHO grade, histology class, IDH mutation, 1p19q status, and MGMT methylation status. This alignment was consistent with previously reported findings. Upon assessment and validation using the CGGA dataset, the risk score exhibited robustness and stability, as evidenced by ROC analysis, Kaplan-Meier survival curves, C-index, and

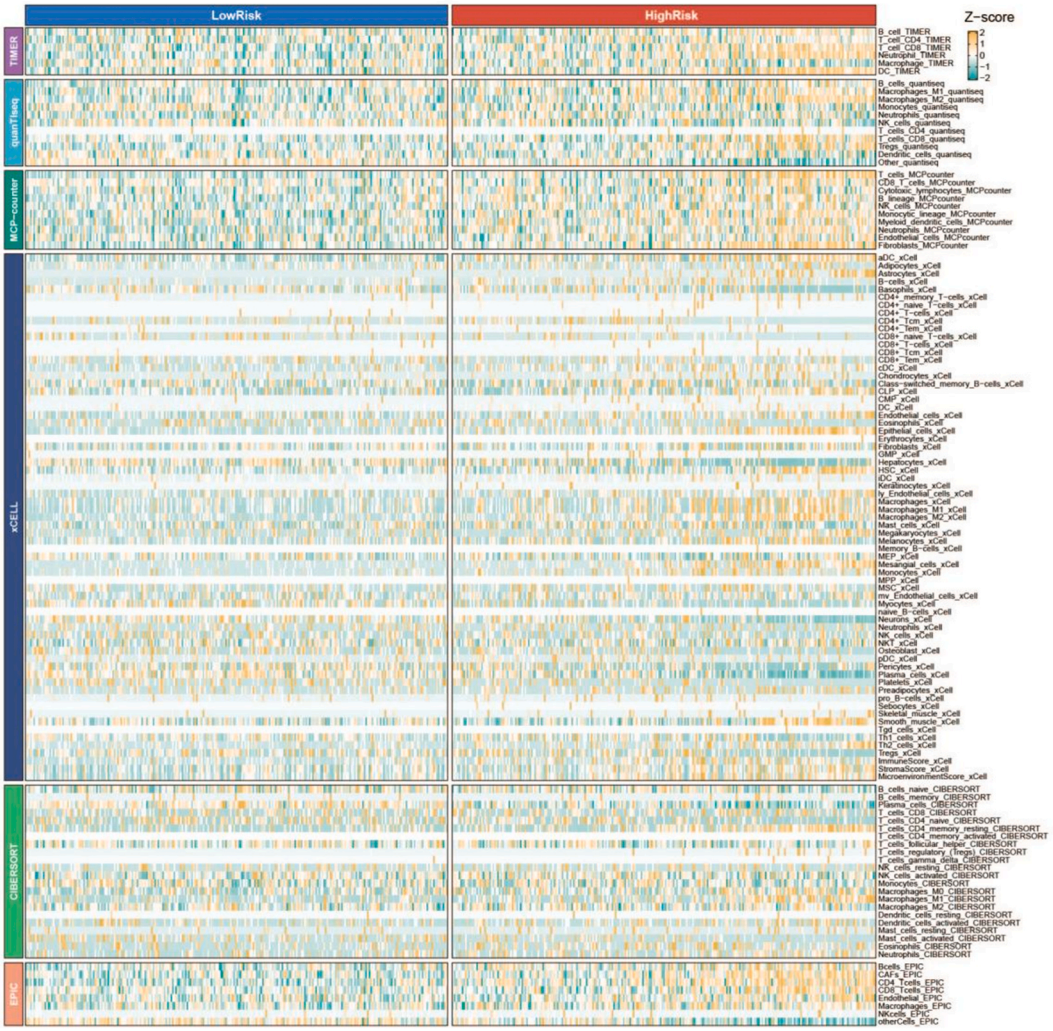

Fig. 12. Immune infiltration between the high- and low-risk score groups using the TIMER, CIBERSORT, quanTIseq, MCP-counter, xCELL and EPIC algorithms.

consensus clustering analysis. Furthermore, the study introduced a constructed nomogram that integrated the risk score with clinical features. This nomogram has the potential to serve as a valuable tool for assessing the survival probability of LGG patients.

Further exploration of the seven model DENGs demonstrated that the expression level of two genes, H2AFX and CASP8, showed a negative correlation with LGG survival. H2AFX holds significance in upholding chromatin structure and genetic stability. Notably, common H2AFX promoter variants could modulate glioma risk, particularly among adults [29]. CASP8, recognized as the initiator caspase of extrinsic apoptosis, concurrently inhibits RIPK3 and MLKL-mediated necroptosis [30]. As a necroptosis inhibitor, CASP8 has been observed to be significantly expressed in gliomas and associated with unfavorable prognoses [31,32].

Five genes, H2AFY2, BID, MAPK10, VDAC2 and GLUD1, were found to positively correlate with LGG survival in our study. H2AFY2, a transcriptional modulator belonging to the H2A histone family, plays a critical role in cell reprogramming, differentiation, and development. It serves as a memory and transcription regulator in the mouse brain [33]. BID, a member of the Bcl-2 family, induces apoptosis and regulates AIF-mediated caspase-independent necroptosis by activating BAX [34,35]. BID and BAX act in concert to trigger apoptosis in glioma cells through the release of mitochondrial cytochrome *c* and subsequent activation of caspases [36]. However, the involvement of H2AFY2 and BID in glioma biology remains uncertain.

GLUD1, a glutamate dehydrogenase, plays a pivotal role in converting glutamate to α-ketoglutaric acid (α-KG) within cancer cells [37]. This enzyme assumes a critical role in redox homeostasis by predominantly governing intracellular α-KG levels in cancer cells [38]. Additionally, GLUD1 is implicated in remodeling the tumor microenvironment within gliomas. Activated GLUD1 augments glutamine metabolism, thereby promoting cell proliferation, colony formation, and tumorigenesis in glioblastoma [39]. MAPK10 (JNK3), a member of the Jun N-terminal kinase (JNK) subfamily of mitogen-activated protein kinases (MAPK), participates in significant physiological processes, including apoptosis [40,41]. Through its phosphorylation and nuclear localization, MAPK10 assumes a regulatory role in signaling pathways during neuronal apoptosis [42]. VDAC2 is a mitochondrial membrane protein, has emerged as

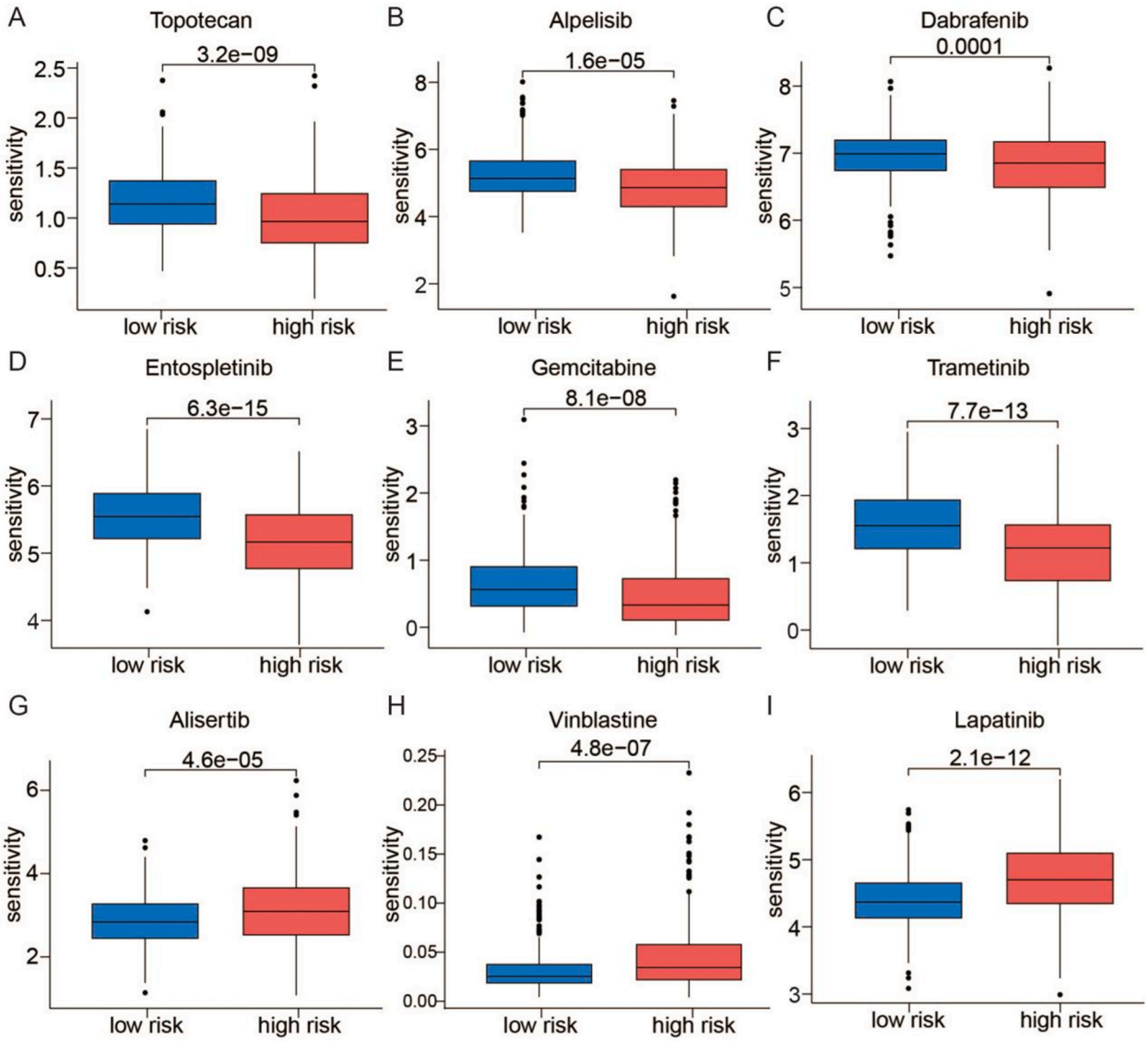

Fig. 13. Examples of drug sensitivity analysis in low and high-risk LGG patients. (A–F) Topotecan, alpelisib, dabrafenib, entospletinib, gemcitabine and trametinib were predicted to be significantly sensitive in the low-risk group. (G–I) Alisertib, vinblastine and lapatinib were predicted to be significantly sensitive in the high-risk group.

a novel regulator of glycolysis. It governs phenotypic switching between glioma stem and non-stem cells, rendering it a potential prognostic marker and therapeutic target for glioma patients [43].

Based on functional enrichment analyses, it is evident that the seven model DENGs potentially partake in embryonic organogenesis, transcriptional regulation, gene activation, and may exert a regulatory role in LGG tumorigenesis through immune and metabolic pathways.

The inflammatory response elicited by necroptosis exhibits a close association with tumor progression [44,45]. The immune system of the CNS possesses a unique character, characterized by a relatively low degree of immune infiltration. Considering that the prognostic DENGs identified within this study predominantly showcased enrichment in immune-related pathways, an evaluation of distinct immune cell infiltrations was conducted to delve into the connection between LGG necroptosis and the tumor immune microenvironment. The results indicated that the high-risk group recruited a higher number of immune cells and induced elevated activation of immune pathways in comparison to the low-risk group. These findings suggest that the model DENGs might play a role in predicting or influencing immunotherapeutic responses among LGG patients. Consequently, the inflammatory cells generated through necroptosis could potentially wield a more significant influence on tumorigenesis by fostering carcinogenesis, inciting the proliferation of cancer cells, and facilitating metastasis.

Beyond immune cell infiltration, the distinctiveness of the glioma tumor microenvironment stands closely linked to the cellular

heterogeneity characteristic of the CNS [46]. Analysis through scRNA-seq unveiled that the identified model DENGs exhibited differential expression across various cell types in LGG. This observation signifies that these DENGs may assume pivotal roles in the oncogenesis of LGG by affecting the biological behavior and function of specific cell populations. However, the precise mechanisms underlying these processes necessitate further investigation in the future.

Discovering potential treatments to aid patients with LGG has consistently stood as a vital objective for researchers. Despite the rapid advancements in tumor immunology that have facilitated our comprehension of LGG, the progress of immunotherapy for this condition remains somewhat unsatisfactory. The analysis of drug sensitivity implies that the attributes of necroptosis-associated genes could offer valuable insights for the selection of anti-cancer drugs in clinical practice. Nevertheless, the dependability of these findings warrants further comprehensive investigations.

Fundings

The study was funded by the National Natural Science Foundation of China (No. 82002663) and the Hainan Provincial Cerebrovascular Disease Clinical Medical Research Center (No. LCYX202107).

Data availability statement

Original data used in this study are publicly available. The TCGA-GTEx combined gene expression dataset (cohort: TCGA TARGET GTEx, RNAseq) and TCGA-LGG dataset (cohort: TCGA Lower Grade Glioma, RNAseq) were downloaded from the UCSC Xena data portal [https://xenabrowser.net/datapages/]. The CGGA-LGG dataset (ID: mRNAseq_693) and scRNA dataset (ID: scRNA-seq) were downloaded from the CGGA database [http://www.cgga.org.cn/download.jsp].

CRediT authorship contribution statement

Xiqi Hu: Data curation, Investigation, Writing – original draft, Writing – review & editing. **Yanan Ma:** Investigation, Writing – original draft, Writing – review & editing. **Ying Xia:** Investigation. **Bo Liu:** Investigation, Project administration, Supervision, Writing – original draft, Writing – review & editing.

Declaration of competing interest

The authors declare that they have no known competing financial interests or personal relationships that could have appeared to influence the work reported in this paper.

Acknowledgements

The authors would like to express their appreciation to the Hainan Cerebrovascular Disease Clinical Research Center Project for their support.

Appendix A. Supplementary data

Supplementary data to this article can be found online at https://doi.org/10.1016/j.heliyon.2023.e23947.

References

[1] P.Y. Wen, R.J. Packer, The 2021 WHO classification of tumors of the central nervous system: clinical implications, Neuro Oncol. 23 (8) (2021) 1215–1217.
[2] A. Perez, J.T. Huse, The evolving classification of diffuse gliomas: world health organization updates for 2021, Curr. Neurol. Neurosci. Rep. 21 (12) (2021) 67.
[3] J. Pallud, et al., Velocity of tumor spontaneous expansion predicts long-term outcomes for diffuse low-grade gliomas, Neuro Oncol. 15 (5) (2013) 595–606.
[4] H. Duffau, L. Taillandier, New concepts in the management of diffuse low-grade glioma: proposal of a multistage and individualized therapeutic approach, Neuro Oncol. 17 (3) (2015) 332–342.
[5] E.S. Murphy, et al., Risk factors for malignant transformation of low-grade glioma, Int. J. Radiat. Oncol. Biol. Phys. 100 (4) (2018) 965–971.
[6] D.E. Christofferson, J. Yuan, Necroptosis as an alternative form of programmed cell death, Curr. Opin. Cell Biol. 22 (2) (2010) 263–268.
[7] W. Dai, et al., The potential role of necroptosis in clinical diseases, Int. J. Mol. Med. 47 (5) (2021) 89.
[8] J. Yan, et al., Necroptosis and tumor progression, Trends Cancer 8 (1) (2022) 21–27.
[9] R. Gupta, et al., Unwinding the modalities of necrosome activation and necroptosis machinery in neurological diseases, Ageing Res. Rev. 86 (2023), 101855.
[10] Y. Ding, et al., MLKL contributes to shikonin-induced glioma cell necroptosis via promotion of chromatinolysis, Cancer Lett. 467 (2019) 58–71.
[11] R. Tang, et al., Ferroptosis, necroptosis, and pyroptosis in anticancer immunity, J. Hematol. Oncol. 13 (1) (2020) 110.
[12] H. Li, et al., PDIA4 correlates with poor prognosis and is a potential biomarker in glioma, OncoTargets Ther. 14 (2021) 125–138.
[13] N. Yatim, et al., RIPK1 and NF-kappaB signaling in dying cells determines cross-priming of CD8(+) T cells, Science 350 (6258) (2015) 328–334.
[14] A. Kaczmarek, P. Vandenabeele, D.V. Krysko, Necroptosis: the release of damage-associated molecular patterns and its physiological relevance, Immunity 38 (2) (2013) 209–223.
[15] S.I. Grivennikov, F.R. Greten, M. Karin, Immunity, inflammation, and cancer, Cell 140 (6) (2010) 883–899.
[16] M.J. Goldman, et al., Visualizing and interpreting cancer genomics data via the Xena platform, Nat. Biotechnol. 38 (6) (2020) 675–678.
[17] X. Shao, et al., scCATCH: automatic annotation on cell types of clusters from single-cell RNA sequencing data, iScience 23 (3) (2020), 100882.

[18] D. Maeser, R.F. Gruener, R.S. Huang, oncoPredict: an R package for predicting in vivo or cancer patient drug response and biomarkers from cell line screening data, Briefings Bioinf. 22 (6) (2021).
[19] N. Cancer Genome Atlas Research, et al., Comprehensive, integrative genomic analysis of diffuse lower-grade gliomas, N. Engl. J. Med. 372 (26) (2015) 2481–2498.
[20] S. Turcan, et al., IDH1 mutation is sufficient to establish the glioma hypermethylator phenotype, Nature 483 (7390) (2012) 479–483.
[21] H. Yan, et al., IDH1 and IDH2 mutations in gliomas, N. Engl. J. Med. 360 (8) (2009) 765–773.
[22] P. Metellus, et al., Absence of IDH mutation identifies a novel radiologic and molecular subtype of WHO grade II gliomas with dismal prognosis, Acta Neuropathol. 120 (6) (2010) 719–729.
[23] P. Wesseling, M. van den Bent, A. Perry, Oligodendroglioma: pathology, molecular mechanisms and markers, Acta Neuropathol. 129 (6) (2015) 809–827.
[24] W. Wick, et al., Long-term analysis of the NOA-04 randomized phase III trial of sequential radiochemotherapy of anaplastic glioma with PCV or temozolomide, Neuro Oncol. 18 (11) (2016) 1529–1537.
[25] M.J. van den Bent, et al., Adjuvant procarbazine, lomustine, and vincristine chemotherapy in newly diagnosed anaplastic oligodendroglioma: long-term follow-up of EORTC brain tumor group study 26951, J. Clin. Oncol. 31 (3) (2013) 344–350.
[26] D.N. Louis, et al., The 2016 world health organization classification of tumors of the central nervous system: a summary, Acta Neuropathol. 131 (6) (2016) 803–820.
[27] M.E. Hegi, et al., MGMT gene silencing and benefit from temozolomide in glioblastoma, N. Engl. J. Med. 352 (10) (2005) 997–1003.
[28] M.R. Gilbert, et al., Dose-dense temozolomide for newly diagnosed glioblastoma: a randomized phase III clinical trial, J. Clin. Oncol. 31 (32) (2013) 4085–4091.
[29] W. Fan, et al., Possible association between genetic variants in the H2AFX promoter region and risk of adult glioma in a Chinese Han population, J. Neuro Oncol. 105 (2) (2011) 211–218.
[30] M. Fritsch, et al., Caspase-8 is the molecular switch for apoptosis, necroptosis and pyroptosis, Nature 575 (7784) (2019) 683–687.
[31] K. Newton, et al., Cleavage of RIPK1 by caspase-8 is crucial for limiting apoptosis and necroptosis, Nature 574 (7778) (2019) 428–431.
[32] S. Wan, et al., Combined bulk RNA-seq and single-cell RNA-seq identifies a necroptosis-related prognostic signature associated with inhibitory immune microenvironment in glioma, Front. Immunol. 13 (2022), 1013094.
[33] Y. Hu, et al., Transcriptional modulator H2A histone family, member Y (H2AFY) marks Huntington disease activity in man and mouse, Proc. Natl. Acad. Sci. U.S. A. 108 (41) (2011) 17141–17146.
[34] L.P. Billen, A. Shamas-Din, D.W. Andrews, Bid: a bax-like BH3 protein, Oncogene 27 (Suppl 1) (2008) S93–S104.
[35] L. Cabon, et al., BID regulates AIF-mediated caspase-independent necroptosis by promoting BAX activation, Cell Death Differ. 19 (2) (2012) 245–256.
[36] M. Bhattacharjee, et al., Bax and Bid act in synergy to bring about T11TS-mediated glioma apoptosis via the release of mitochondrial cytochrome c and subsequent caspase activation, Int. Immunol. 20 (12) (2008) 1489–1505.
[37] Y.Q. Wang, et al., Sirtuin5 contributes to colorectal carcinogenesis by enhancing glutaminolysis in a deglutarylation-dependent manner, Nat. Commun. 9 (1) (2018) 545.
[38] L. Jin, et al., Glutamate dehydrogenase 1 signals through antioxidant glutathione peroxidase 1 to regulate redox homeostasis and tumor growth, Cancer Cell 27 (2) (2015) 257–270.
[39] R. Yang, et al., EGFR activates GDH1 transcription to promote glutamine metabolism through MEK/ERK/ELK1 pathway in glioblastoma, Oncogene 39 (14) (2020) 2975–2986.
[40] C. Tournier, et al., Requirement of JNK for stress-induced activation of the cytochrome c-mediated death pathway, Science 288 (5467) (2000) 870–874.
[41] D.D. Yang, et al., Absence of excitotoxicity-induced apoptosis in the hippocampus of mice lacking the Jnk3 gene, Nature 389 (6653) (1997) 865–870.
[42] H. Matsuura, et al., Phosphorylation-dependent scaffolding role of JSAP1/JIP3 in the ASK1-JNK signaling pathway. A new mode of regulation of the MAP kinase cascade, J. Biol. Chem. 277 (43) (2002) 40703–40709.
[43] K. Zhou, et al., VDAC2 interacts with PFKP to regulate glucose metabolism and phenotypic reprogramming of glioma stem cells, Cell Death Dis. 9 (10) (2018) 988.
[44] I.L. Ch'en, et al., Mechanisms of necroptosis in T cells, J. Exp. Med. 208 (4) (2011) 633–641.
[45] M. Pasparakis, P. Vandenabeele, Necroptosis and its role in inflammation, Nature 517 (7534) (2015) 311–320.
[46] A. Gieryng, et al., Immune microenvironment of gliomas, Lab. Invest. 97 (5) (2017) 498–518.